Journal of Biomedical Optics

BiomedicalOptics.SPIEDigitalLibrary.org

Quantitative photoacoustic tomography using illuminations from a single direction

Aki Pulkkinen
Ben T. Cox
Simon R. Arridge
Jari P. Kaipio
Tanja Tarvainen

SPIE.

Quantitative photoacoustic tomography using illuminations from a single direction

Aki Pulkkinen,[a,*] Ben T. Cox,[b] Simon R. Arridge,[c] Jari P. Kaipio,[a,d] and Tanja Tarvainen[a,c]
[a]University of Eastern Finland, Department of Applied Physics, P.O. Box 1627, 70211 Kuopio, Finland
[b]University College London, Department of Medical Physics and Bioengineering, Gower Street, London WC1E 6BT, United Kingdom
[c]University College London, Department of Computer Science, Gower Street, London WC1E 6BT, United Kingdom
[d]Department of Mathematics at University of Auckland, and Dodd-Walls Centre for Photonic and Quantum Technologies, Private Bag 92019, Auckland Mail Centre, Auckland 1142, New Zealand

Abstract. Quantitative photoacoustic tomography is an emerging imaging technique aimed at estimating optical parameters inside tissues from photoacoustic images, which are formed by combining optical information and ultrasonic propagation. This optical parameter estimation problem is ill-posed and needs to be approached within the framework of inverse problems. It has been shown that, in general, estimating the spatial distribution of more than one optical parameter is a nonunique problem unless more than one illumination pattern is used. Generally, this is overcome by illuminating the target from various directions. However, in some cases, for example when thick samples are investigated, illuminating the target from different directions may not be possible. In this work, the use of spatially modulated illumination patterns at one side of the target is investigated with simulations. The results show that the spatially modulated illumination patterns from a single direction could be used to provide multiple illuminations for quantitative photoacoustic tomography. Furthermore, the results show that the approach can be used to distinguish absorption and scattering inclusions located near the surface of the target. However, when compared to a full multidirection illumination setup, the approach cannot be used to image as deep inside tissues. [DOI: 10.1117/1.JBO.20.3.036015]

Keywords: photoacoustics; inverse problems; image reconstruction; radiative transfer.

Paper 140853R received Dec. 23, 2014; accepted for publication Mar. 6, 2015; published online Mar. 24, 2015.

1 Introduction

Photoacoustic tomography (PAT) is an emerging imaging modality developed over the last two decades, which combines the benefits of optical contrast and ultrasound propagation. The optical aspect provides information on the distribution of chromophores, which are light-absorbing molecules within the tissue. The chromophores of interest are, for example, haemoglobin, melanin, and various contrast agents. The ultrasonic waves carry this optical information directly to the surface with minimal scattering, thus retaining accurate spatial information as well. Nowadays, PAT can be used to provide images of soft biological tissues with high spatial resolution. It has successfully been applied to the visualization of different structures in biological tissues, such as human blood vessels, microvasculature of tumors, and the cerebral cortex in small animals. However, this information is only a qualitative image and it does not include quantitative information on the concentrations of the chromophores. For more information about PAT, see, for example, Refs. 1–5 and the references therein.

Quantitative photoacoustic tomography (QPAT) is a technique aimed at estimating the absolute concentrations of the chromophores.[6] This is a hybrid imaging problem in which the solution of one inverse problem acts as data for another ill-posed inverse problem. The first inverse problem of QPAT is to reconstruct the initial acoustic pressure distribution from the measured acoustic waves. This is an inverse initial value problem in acoustics, and there are a large number of reconstruction techniques available, see, for example, Refs. 1, 3, and 7 and the references therein. However, in cases in which the speed of sound and acoustic absorption within the tissue are spatially varying, the inverse problem becomes significantly more challenging.[8–17] In this paper, it is assumed that the acoustic inverse problem in QPAT is performed in an idealistic fashion. The data that are utilized in the numerical analysis are formed by using the true acoustic initial pressure distribution with noise added to it. In practice, however, the data would be the solution of the acoustic inverse problem. Therefore, although not discussed in this work, issues related to an acoustic inverse problem, such as sensor response, (limited view) measurement geometry, etc., need to be solved. For potential solutions, see, for example, Refs. 18–23 and the references therein.

The second inverse problem in QPAT is the optical image reconstruction problem of reconstructing the distributions of the optical parameters from the absorbed optical energy density. The goal is to estimate the concentrations of chromophores. These can be obtained either by directly estimating the distributions of concentrations at various wavelengths[6,24–31] or by first recovering the absorption coefficients at different wavelengths and then calculating the concentrations from the absorption spectra.[6] In order to obtain accurate estimates, the scattering effects also need to be taken into account.[6,32–34]

In the optical inverse problem of QPAT, in the absence of other suitable prior knowledge, estimation of both absorption

*Address all correspondence to: Aki Pulkkinen, E-mail: aki.pulkkinen@uef.fi

and scattering is generally nonunique if only one light illumination is used.[30,32] To overcome this problem, one approach has been to assume the scattering as known and to estimate only the absorption.[35–40] This, however, is unrealistic since in practical applications scattering is usually not exactly known. This approach has been improved by modeling the errors caused by the fixed scattering assumption by using a Bayesian approximation error modeling.[34] As an alternative approach, in Ref. 41, the absorption and the photon fluence were extracted using a sparse signal representation, and the inverse problem was formulated as a problem of finding boundaries between the piecewise constant optical parameters in Ref. 42.

In Ref. 32, it was shown that the nonuniqueness can be overcome by using multiple optical illuminations. Generally, this has been achieved by illuminating the target from different directions.[30,32,33,43–47] Also, combining QPAT and diffuse optical tomography (DOT) data types can be used to overcome the nonuniqueness.[48,49] However, in some cases, for example when thick samples are investigated, illuminating the target from different directions may not be possible.

In this work, multiple illuminations are provided by using spatially modulated illumination patterns at one side of the target. Using spatially modulated light patterns have been previously investigated in the case of other near-infrared light based imaging modalities to improve the quality of the reconstructed images. In DOT, fluorescence DOT and combined DOT-QPAT multiple light patterns have been utilized to reduce the ill-posedness and to improve the spatial resolution of the reconstructed images.[48,50–53] Furthermore, optimal source patterns that would maximize the detectivity of the inhomogeneities in DOT have been investigated.[54] In the case of QPAT, good spatial resolution is provided by the ultrasound propagation. On the other hand, the multiple light patterns can be used to overcome the nonuniqueness problem of the illumination from a single side. The approach can be expected to be valid as deep in the medium as the light patterns are distinguishable, which depends on the optical properties of the target.

In this work, simultaneous estimation of absorption and scattering in QPAT using multiple illumination patterns originating from a single direction of the target is investigated. The work is motivated by measurement setups that can be limited to one side of the target.[55] The image reconstruction problem is approached in the Bayesian framework for ill-posed inverse problems.[31,34,56–58]

Due to the ill-posedness of the optical inverse problem of QPAT, the reconstruction is sensitive to measurement and modeling errors. Therefore, light propagation within the target needs to be accurately modeled. In this case, when illuminations are provided only from a single direction, the imaging regions are thin, and thus, the radiative transfer equation (RTE) needs to be used as the model for light propagation.[30,33,47,59]

The rest of the paper is organized as follows. The optical image reconstruction in QPAT and the proposed approach are described in Sec. 2. The results of simulations are shown in Sec. 3, and the conclusions are given in Sec. 4.

2 Methods

In QPAT, a short pulse of near-infrared light is used to illuminate the region of interest. As light propagates within the tissue, it is absorbed by chromophores. This generates localized increases in pressure. This pressure increase propagates through the tissue as an acoustic wave and is detected by ultrasound sensors on the surface of the tissue. The propagation of the acoustic wave occurs on a microsecond time scale, about five orders of magnitude slower than the optical propagation, so only the total absorbed optical energy density is of interest and not the rate of the absorption. This large difference in the time scales allows the optical and acoustic parts of the inverse problem to be decoupled and treated separately. In this work, the optical inverse problem of QPAT is considered.

In the optical inverse problem of QPAT, the discretized distribution of the optical parameters inside the object is estimated when the absorbed optical energy density $\mathcal{H}_{\text{meas}}$ is given. In this paper, the optical parameters of interest are the absorption and scattering coefficients, and the inverse problem is solved with a Bayesian inverse problems approach.[56] Thus, one seeks to find the distribution of the optical parameters $(\hat{\mu}_a, \hat{\mu}_s)$, which minimizes the functional

$$(\hat{\mu}_a, \hat{\mu}_s) = \underset{(\mu_a,\mu_s)}{\operatorname{argmin}} \|L_e[\mathcal{H}_{\text{meas}} - H(\mu_a, \mu_s) - \eta_e]\|^2 + \|L_{\mu_a}(\mu_a - \eta_{\mu_a})\|^2 + \|L_{\mu_s}(\mu_s - \eta_{\mu_s})\|^2, \quad (1)$$

where $\mathcal{H}_{\text{meas}}$ and H are the measured and the modeled absorbed optical energy density, respectively, η_e, η_{μ_a}, and η_{μ_s} are the means of the noise and the priors for absorption and scattering, and $L_e^T L_e = \Gamma_e^{-1}$, $L_{\mu_a}^T L_{\mu_a} = \Gamma_{\mu_a}^{-1}$, and $L_{\mu_s}^T L_{\mu_s} = \Gamma_{\mu_s}^{-1}$ are the Cholesky decompositions of the inverse covariance matrices of the probability distributions representing the noise and the prior. Equation (1) describes the maximum *a posteriori* estimate of the inverse problem, where it is presumed that the statistics of the noise and the prior information of the parameters of interest can be presented using Gaussian distributions. In this work, the minimization problem [Eq. (1)] is solved using a Gauss-Newton method equipped with a line search algorithm and a positivity constraint.

2.1 *Light Propagation Model*

Let $\Omega \subset \mathbb{R}^n$, $n = 2$ or 3, denote the physical domain with boundary $\partial\Omega$ and let $s \in S^{n-1}$ denote a unit vector of the direction of light propagation. In this paper, the propagation of light is modeled using the time-independent RTE

$$s \cdot \nabla\phi(r,s) + (\mu_a + \mu_s)\phi(r,s) = \mu_s \int_{S^{n-1}} \Theta(s \cdot s')\phi(r,s')\mathrm{d}s', \quad (2)$$

where $\phi(r,s)$ is the radiance at the position $r \in \Omega$ into the direction s, μ_a and μ_s are the (spatially varying) absorption and scattering parameters, and $\Theta(s \cdot s')$ is the scattering phase function describing the probability of light scattering from direction s' to direction s. A vacuum type boundary condition for the RTE [Eq. (2)] is used and it takes the form

$$\phi(r,s) = \phi_0(r,s), \quad r \in \partial\Omega, \quad s \cdot \nu \le 0, \quad (3)$$

where ν is the outward normal on $\partial\Omega$, and $\phi_0(r,s)$ describes the inward radiance on the boundary (i.e., the light source). In this work, the solution of the RTE [Eq. (2)] is numerically approximated using a finite element method with piecewise linear representations of both spatial and angular discretizations and the optical parameters.[33,60] For the scattering phase function Θ, the Henyey-Greenstein scattering function is used.[61]

The absorption of light results in the absorbed optical energy density field

$$H(r) = \mu_a(r)\Phi(r), \tag{4}$$

where Φ is the fluence obtained from the radiance

$$\Phi(r) = \int_{S^{n-1}} \phi(r,s)\mathrm{d}s. \tag{5}$$

2.2 *Light Illuminations*

In this work, a two-dimensional ($n = 2$) rectangular domain Ω, with coordinates spanning $[-2.5\ \mathrm{mm}, 2.5\ \mathrm{mm}] \times [-5\ \mathrm{mm}, 5\ \mathrm{mm}]$, is investigated. Two types of light illumination patterns are studied: the single-direction and the multidirection illuminations. For both illumination types, two different spatial modulations of light are used. In the single-direction illumination patterns, light is set to enter the target only from one side of it. In the multidirection illuminations, light enters the target from various sides. The two different inward radiances of the single-direction illuminations are defined as

$$\phi_{0,1}(r,s) = \begin{cases} -(s\cdot\nu)\left[1-\cos\left(\frac{2\pi}{5\ \mathrm{mm}}y\right)\right]^2, & r\in\partial\Omega_L, \quad s\cdot\nu\le 0 \\ 0, & r\in\partial\Omega_R\cup\partial\Omega_B\cup\partial\Omega_T, \quad s\cdot\nu\le 0 \end{cases}$$
$$\phi_{0,2}(r,s) = \begin{cases} -(s\cdot\nu)\left[1+\cos\left(\frac{3\pi}{5\ \mathrm{mm}}y\right)\right]^2, & r\in\partial\Omega_L, \quad s\cdot\nu\le 0 \\ 0, & r\in\partial\Omega_R\cup\partial\Omega_B\cup\partial\Omega_T, \quad s\cdot\nu\le 0 \end{cases}, \tag{6}$$

where ν is the outward normal at the boundary, $\partial\Omega_L$, $\partial\Omega_R$, $\partial\Omega_T$, and $\partial\Omega_B$ correspond to left, right, top, and bottom boundaries of the rectangular domain Ω, and $y \in [-5\ \mathrm{mm}, 5\ \mathrm{mm}]$ is the vertical coordinate. The factors $[1-\cos(2\pi y/5\ \mathrm{mm})]^2$ and $[1+\cos(3\pi y/5\ \mathrm{mm})]^2$ produce a positive inward radiance with sinusoidal spatial modulation on the left side of the rectangular domain. For the multidirection illuminations, the inward radiances are defined as

$$\phi_{0,1}(r,s) = \begin{cases} -s\cdot\nu, & r\in\partial\Omega_L\cup\partial\Omega_T, \quad s\cdot\nu\le 0 \\ 0, & r\in\partial\Omega_R\cup\partial\Omega_B, \quad s\cdot\nu\le 0 \end{cases}$$
$$\phi_{0,2}(r,s) = \begin{cases} 0, & r\in\partial\Omega_L\cup\partial\Omega_T, \quad s\cdot\nu\le 0 \\ -s\cdot\nu, & r\in\partial\Omega_R\cup\partial\Omega_B, \quad s\cdot\nu\le 0 \end{cases}. \tag{7}$$

In this work, both single- and multidirection illuminations have a sinusoidal inward angular directivity pattern for the radiance, given by the factor $-(s\cdot\nu)$ in Eqs. (6) and (7). This means that the light source is such that no light is transmitted parallel to the surface while maximum transmission takes place perpendicular to the surface, thus mimicking the behavior of a light source with a directional radiation pattern as could be used in QPAT.

An example of fluence distribution inside the domain with homogeneous optical parameters corresponding to the background parameter values used in the simulations in Sec. 3 is shown in Fig. 1. As can be seen, the spatial patterns between the two single-direction illuminations are clearly distinguishable only close to the surface of the illumination direction (the left edge), with the fluence patterns becoming indistinguishable deeper in the domain. This becomes more apparent when comparing the contour lines produced by the two spatial illumination patterns, which come close to overlapping deeper in the target. For the multidirection illumination patterns, the fluence is clearly distinguishable between the two illumination patterns throughout the domain.

3 Results

The simulations were performed in a rectangular two-dimensional domain of size 5 mm × 10 mm. Two problems were investigated: one in which the noise level was varied, and the second in which the location (depth) of the inclusions (variations of μ_a and μ_s from the background value) within the simulation domain was varied.

3.1 *Data Simulation*

The data were simulated using the RTE [Eq. (2)] together with the boundary condition [Eq. (3)]. Two single-direction illumination patterns were created according to Eq. (6). For comparison, data using multidirection illuminations [Eq. (7)] were created. In all of the simulations, the Henyey-Greenstein scattering anisotropy value $g = 0.9$ was used. In all cases, the spatial finite element discretization consisted of 6492 triangular elements with 3355 grid-nodes, and an angular discretization of 32 directions was used. The fluence and absorbed optical energy density were calculated from the radiance using Eqs. (4) and (5).

The resulting absorbed energy density fields were then interpolated into the inversion grid composed of 5690 triangular elements with 2947 grid-nodes and 32 angular directions. After the interpolation, normally distributed zero-mean noise with a standard deviation proportional to the absorbed energy density field was added to the data as

$$\mathcal{H}_{\mathrm{meas}} = (1+\epsilon\xi)\mathcal{H}, \tag{8}$$

where ξ is normally distibuted noise with a zero mean and standard deviation of one, ϵ is the noise amplitude, and $\mathcal{H}$ is the simulated noiseless absorbed energy density field. Values of ϵ of 0.05, 0.01, and 0.001 were used.

3.2 *Reconstructions*

Absorption and scattering distibution were estimated by minimizing Eq. (1). For the noise statistics, accurate parameters of zero mean and covariance matrix $\Gamma_e = \mathrm{diag}\{\epsilon^2\mathcal{H}^2\}$ were

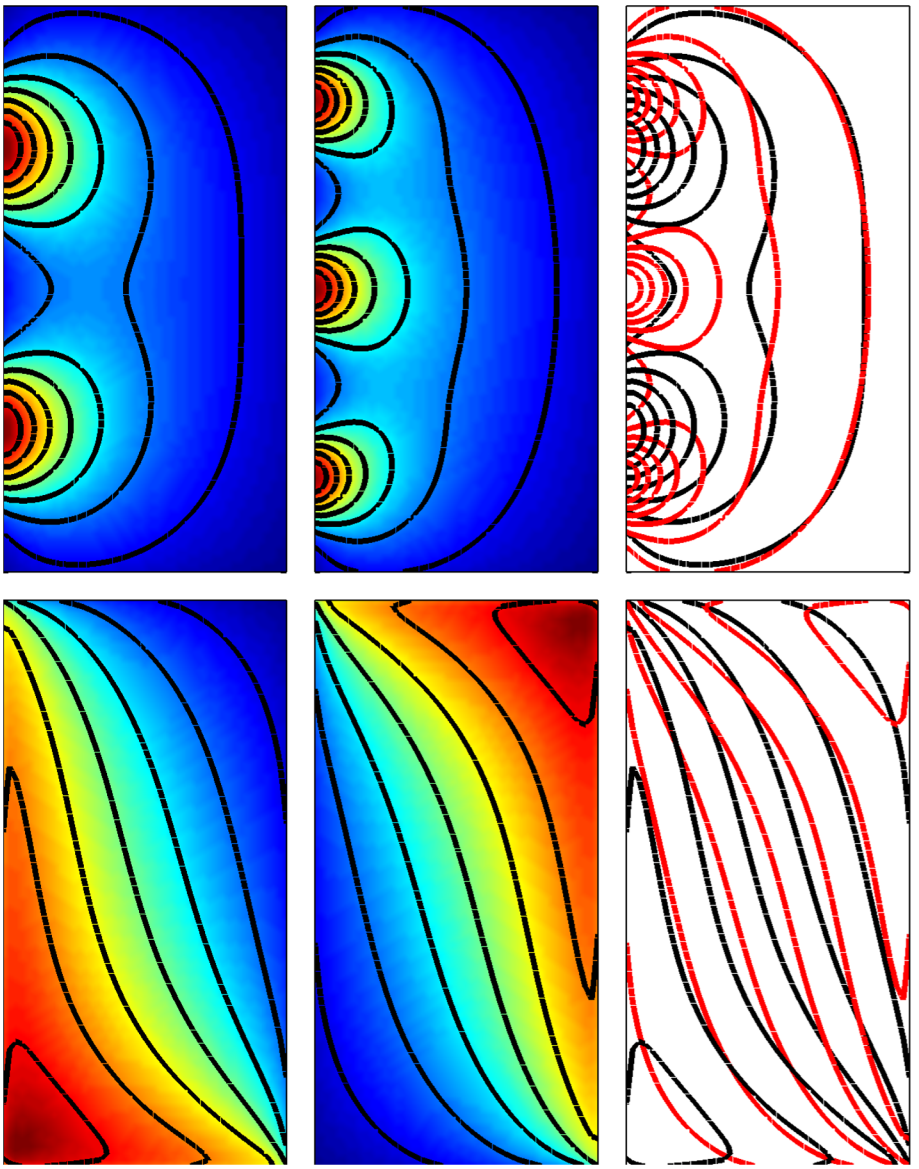

Fig. 1 Fluence distributions for single- and multidirection light sources given by Eqs. (6) and (7) shown in the top and bottom rows, respectively. Fluence shown in 5 mm × 10 mm domain. The left and middle column show the fluence for inward radiances $\phi_{0,1}$ and $\phi_{0,2}$, respectively. The seven solid lines denote contour lines of constant fluence for 87.5, 75.0, 62.5, 50.0, 37.5, 25.0, and 12.5% of the peak fluence. The right column shows the contour lines for light sources $\phi_{0,1}$ and $\phi_{0,2}$ with black and red lines, respectively.

used. As the prior model of the unknown μ_a and μ_s, an Ornstein-Uhlenbeck process derived statistics was chosen,[62] which has previously been used in a Bayesian inverse problem approach in QPAT.[31] Accordingly, the marginal covariance matrices of the prior was set as being proportional to matrix Ξ with its elements defined as

$$\Xi_{ij} = \exp(-\|r_i - r_j\|/l), \tag{9}$$

where r_i and r_j are the coordinates r of the i'th and j'th grid-node and l is the correlation distance set to $l = 1$ mm. The correlation distance was arbitrarily chosen to support distributions with distinguishable spatial features within the investigated domain size. The choice is a compromise, as choosing a very short correlation distance would result in an almost white noise behavior of the prior supporting spatially uncorrelated features in the estimates. On the other hand, choosing a long correlation distance could bias the estimates to have minimal spatial features. The prior statistics for μ_a and μ_s were defined as $\mu_a \sim \mathcal{N}(\eta_{\mu_a}, \Gamma_{\mu_a})$ and $\mu_s \sim \mathcal{N}(\eta_{\mu_s}, \Gamma_{\mu_s})$, with

$$\begin{aligned}
\eta_{\mu_a} &= \frac{1}{2}(\max\ \mu_a + \min\ \mu_a),\\
\Gamma_{\mu_a} &= \frac{1}{4}(\max\ \mu_a - \min\ \mu_a)^2\Xi,\\
\eta_{\mu_s} &= \frac{1}{2}(\max\ \mu_s + \min\ \mu_s),\\
\Gamma_{\mu_s} &= \frac{1}{4}(\max\ \mu_s - \min\ \mu_s)^2\Xi,
\end{aligned} \tag{10}$$

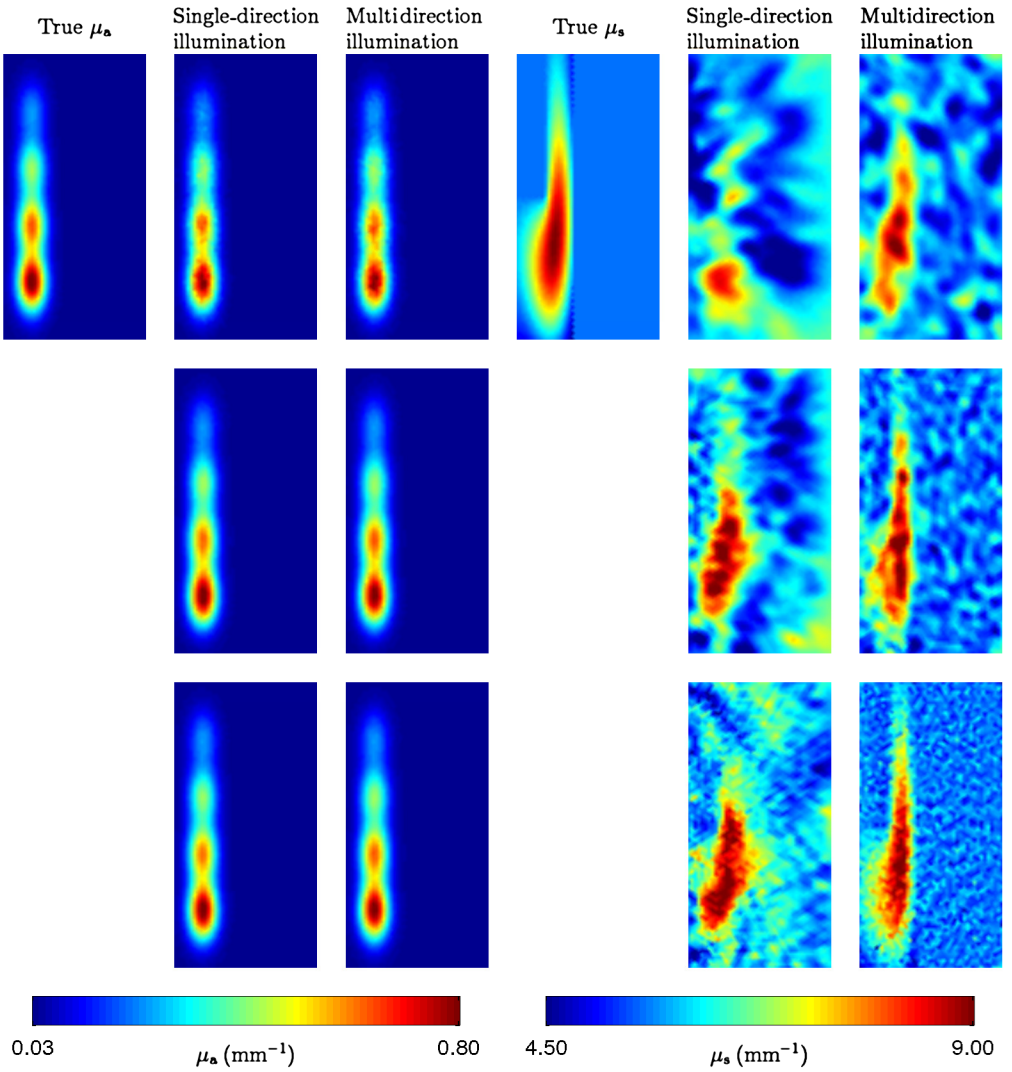

Fig. 2 Optical absorption and scattering parameters μ_a and μ_s used to simulate the data with the inclusions located at a depth of $d = 1$ mm, and their reconstructions with the single- and multidirection illuminations. Reconstructions shown for three noise levels (from top to bottom): $\epsilon = 0.05$, $\epsilon = 0.01$, and $\epsilon = 0.001$.

where min μ_a, max μ_a, min μ_s, and max μ_s are the assumed low and high values of the range of variation of the optical absorption and scattering parameters, and it has been assumed that the parameters vary by one standard deviation from the midpoint of the ranges. For min μ_a, max μ_a, min μ_s, and max μ_s, the true minimum and maximum values of the optical absorption and scattering parameters were used.

Quantification of the accuracy of the reconstructions was evaluated in terms of the relative error of μ_a and μ_s with

$$E_{\mu_a} = 100\% \cdot \frac{\|\mu_{a,\mathrm{TRUE}} - \hat{\mu}_a\|}{\|\mu_{a,\mathrm{TRUE}}\|},$$
$$E_{\mu_s} = 100\% \cdot \frac{\|\mu_{s,\mathrm{TRUE}} - \hat{\mu}_s\|}{\|\mu_{s,\mathrm{TRUE}}\|}, \quad (11)$$

where $\mu_{a,\mathrm{TRUE}}$ and $\mu_{s,\mathrm{TRUE}}$ are the true (simulated) optical absorption and scattering, and $\hat{\mu}_a$ and $\hat{\mu}_s$ are the estimated absorption and scattering obtained with Eq. (1).

Table 1 Relative errors of the absorption and scattering estimates, E_{μ_a} and E_{μ_s}, for the single- and multidirection illuminations. Relative errors shown for noise level variations of Sec. 3.3 (noise level 1 to 3) and inclusion depth variations of Sec. 3.4 (depth 1 to 4).

	E_{μ_a} (%)		E_{μ_s} (%)	
Simulation	Single	Multi	Single	Multi
Noise level 1 ($\epsilon = 0.05$, $d = 1$ mm)	4.38	3.63	12.79	8.43
Noise level 2 ($\epsilon = 0.01$, $d = 1$ mm)	2.06	0.80	10.26	6.07
Noise level 3 ($\epsilon = 0.001$, $d = 1$ mm)	2.07	0.21	11.11	4.87
Depth 1 ($\epsilon = 0.01$, $d = 1$ mm)	1.47	0.80	11.08	6.12
Depth 2 ($\epsilon = 0.01$, $d = 2$ mm)	5.37	0.76	13.02	6.15
Depth 3 ($\epsilon = 0.01$, $d = 3$ mm)	5.72	0.74	12.36	6.25
Depth 4 ($\epsilon = 0.01$, $d = 4$ mm)	3.20	0.77	14.37	6.02

3.3 *Noise-Level Variations*

First, the impact of the noise level on the accuracy of the estimates was investigated. Three noise levels, $\epsilon = 0.05$, $\epsilon = 0.01$, and $\epsilon = 0.001$, were used when the data were simulated. True absorption and scattering parameters used to simulate the data are shown in Fig. 2. The true absorption and scattering inclusions were located approximately at a depth of $d = 1$ mm. Estimated absorption and scattering distributions are shown in Fig. 2.

Qualitatively, the absorption estimates match the true absorption well, with small ripples visible in the reconstructions with the highest noise level. The differences between the single- and multidirection illuminations become more apparent in the estimates of scattering coefficients. It can be seen that the single-direction illuminations result in an overall worse visual quality of the scattering reconstructions than the multidirection illuminations, as the size and shape of the scattering inclusion are more distorted in the reconstructions. An improvement in the

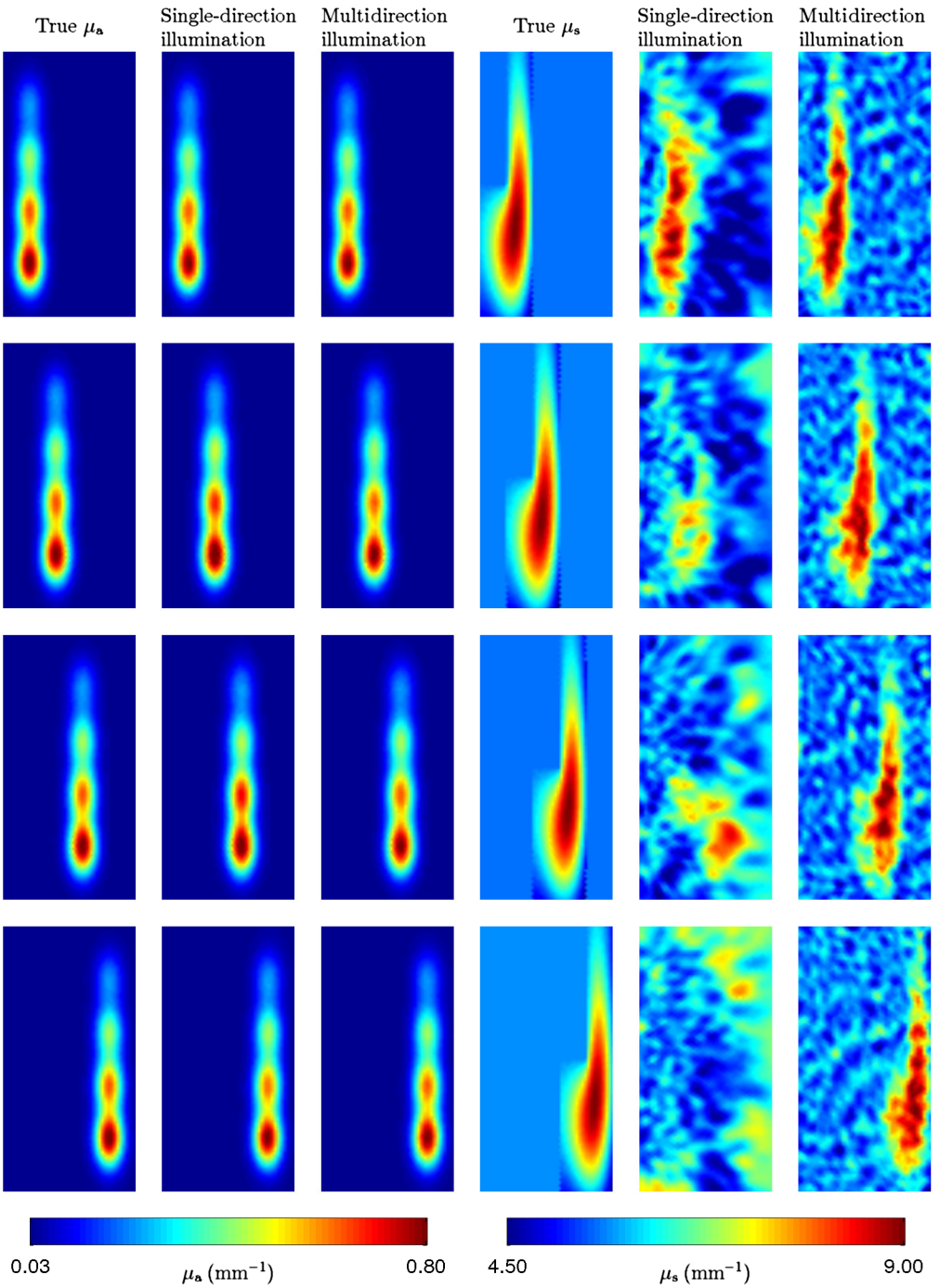

Fig. 3 Optical absorption and scattering parameters μ_a and μ_s used to simulate the data, and their reconstructions with the single- and multidirection illuminations. Parameters and reconstructions shown for four depths of the inclusions $d = 1$ mm, 2 mm, 3 mm, and 4 mm (from top to bottom). Reconstructions are shown for the noise level $\epsilon = 0.01$.

visual quality of the reconstruction is evident when the noise level is reduced.

Table 1 shows the relative errors of the reconstructions computed using Eq. (11). As can be seen, both the absorption and scattering estimates using single-direction illuminations are more sensitive to noise than the estimates using multidirection illuminations since their relative errors are higher than those using the multidirection illuminations. An improvement of the estimates takes place when the noise level is reduced for both the single- and multidirection illuminations. However, the relative errors using the single-direction illumination do not change significantly when the error level is reduced from $\epsilon = 0.01$ to $\epsilon = 0.001$.

The single-direction reconstructions in comparison to multidirection reference reconstructions show that, in order to obtain equally accurate reconstructions with single-direction illuminations, the measurement system (and the acoustic solution method) has to have a lower noise level than when using a system capable of multidirection illuminations.

3.4 *Inclusion-Depth Variations*

The depth of the absorption and scattering inclusions was varied from the edge of the simulation domain. Figure 3 shows the optical absorption and scattering parameters used in the simulations for inclusion depths of $d = 1$ mm, 2 mm, 3 mm, and 4 mm. Both single- and multidirection illuminations were used to simulate the data using the noise level $\epsilon = 0.01$.

The estimated absorption and scattering distributions are shown in Fig. 3. As can be seen, the absorption reconstructions look visually equally good at all the investigated depths for both single- and multidirection illuminations. However, for the scattering reconstructions obtained using the single-direction illuminations, it can be seen that estimates are worse the deeper the inclusions are from the light source, and no resemblance to the true scattering distribution is observed except when the inclusions are located close to the light source. When the multidirection illuminations are used, the scattering reconstructions are qualitatively equally good regardless of the depth of inclusions.

The relative errors of the absorption and scattering estimates are shown in Table 1. The relative errors when using single-direction illuminations become higher as the depth of the inclusions is increased. The relative errors obtained using multidirection illuminations are similar to each other for all inclusion depths.

The single-direction reconstructions in comparison to the multidirection reference reconstructions show that it is possible to obtain both qualitative and quantitative information on the absorption. However, when using single-direction illuminations, the information regarding the optical scattering is lost rapidly as a function of depth due to the attenuation of the fluence.

4 Conclusions

In this work, QPAT using single-direction illuminations was investigated. Simultaneous estimation of the absorption and scattering distributions was considered. The image reconstruction in QPAT is an ill-posed problem, and therefore, it needs to be approached in the framework of inverse problems. The problem is also known to be generally nonunique unless more than one optical illumination or other additional information is utilized.[27,30,32,42,48] In this work, multiple spatially modulated illuminations originating from one direction of the target were used in order to overcome the nonuniqueness of the reconstruction problem. The RTE was used as the model for light propagation. The approach was tested with simulations.

The simulations suggest that, when compared to the multidirection reference reconstructions, in order to obtain equally accurate reconstructions with single-direction illuminations, the data must have a lower noise level. It was also shown that when using single-direction illuminations, the information regarding the optical scattering is quickly lost (as a function of depth) due to the attenuation of fluence. However, it is possible to obtain both qualitative and quantitative information on the absorption using single-direction illuminations even when information on the scattering is lost. This is significant, since in biological optical imaging, the optical absorption is more important than the scattering. Thus, reconstruction of both absorption and scattering in QPAT is possible using single-direction illuminations when spatially varying illumination patterns are used. However, the quality requirements of the measurement system (and the acoustic inverse problem solution method) are much higher and the approach is not able to image as deep inside the tissue when compared to a setup capable of multidirection illuminations.

Acknowledgments

This work has been supported by the Academy of Finland (projects 136220, 140984, 272803, and 250215 Finnish Centre of Excellence in Inverse Problems Research), the strategic funding of the University of Eastern Finland, and by EPSRC grant EP/K009745/1.

References

1. M. Xu and L. V. Wang, "Photoacoustic imaging in biomedicine," *Rev. Sci. Instrum.* **77**, 041101 (2006).
2. C. Li and L. V. Wang, "Photoacoustic tomography and sensing in biomedicine," *Phys. Med. Biol.* **54**, R59–R97 (2009).
3. L. V. Wang, Ed., *Photoacoustic Imaging and Spectroscopy*, CRC Press, Florida (2009).
4. P. Beard, "Biomedical photoacoustic imaging," *Interface Focus* **1**(4), 602–631 (2011).
5. J. Xia and L. V. Wang, "Small-animal whole-body photoacoustic tomography: a review," *Phys. Med. Biol.* **61**(5), 1380–1389 (2014).
6. B. Cox et al., "Quantitative spectroscopic photoacoustic imaging: a review," *J. Biomed. Opt.* **17**(6), 061202 (2012).
7. P. Kuchment and L. Kunyansky, "Mathematics of thermoacoustic tomography," *Eur. J. Appl. Math.* **19**, 191–224 (2008).
8. X. Jin and L. Wang, "Thermoacoustic tomography with correction for acoustic speed variations," *Phys. Med. Biol.* **51**, 6437–6448 (2006).
9. Y. Hristova, P. Kuchment, and L. Nguyen, "Reconstruction and time reversal in thermoacoustic tomography in acoustically homogeneous and inhomogeneous media," *Inverse Probl.* **24**, 055006 (2008).
10. C. Zhang and Y. Wang, "A reconstruction algorithm for thermoacoustic tomography with compensation for acoustic speed heterogeneity," *Phys. Med. Biol.* **53**, 4971–4982 (2008).
11. R. Kowar and O. Scherzer, "Photoacoustic imaging taking into account attenuation," arXiv: 1009.4350 [math.AP].
12. B. T. Cox and B. E. Treeby, "Artifact trapping during time reversal photoacoustic imaging for acoustically heterogeneous media," *IEEE Trans. Med. Imaging* **29**(2), 387–396 (2010).
13. B. E. Treeby, E. Z. Zhang, and B. T. Cox, "Photoacoustic tomography in absorbing acoustic media using time reversal," *Inverse Probl.* **26**, 115003 (2010).
14. X. L. Deán-Ben et al., "Statistical approach for optoacoustic image reconstruction in the presence of strong acoustic heterogeneities," *IEEE Trans. Med. Imaging* **30**(2), 401–408 (2011).
15. R. W. Schoonover and M. A. Anastasio, "Compensation of shear waves in photoacoustic tomography with layered acoustic media," *J. Opt. Soc. Am. A* **28**(10), 2091–2099 (2011).

16. R. W. Schoonover, L. V. Wang, and M. A. Anastasio, "Numerical investigation of the effects of shear waves in transcranial photoacoustic tomography with a planar geometry," *J. Biomed. Opt.* **17**(6), 061215 (2012).
17. C. Huang et al., "Photoacoustic computed tomography correcting for heterogeneity and attenuation," *J. Biomed. Opt.* **17**(6), 061211 (2012).
18. M. A. Anastasio et al., "Improving limited-view reconstruction in photoacoustic tomography by incorporating a priori boundary information," *Proc. SPIE* **6856**, 68561B (2008).
19. A. Buehler et al., "Model-based optoacoustic inversions with incomplete projection data," *Med. Phys.* **38**(3), 1694–1704 (2011).
20. B. T. Cox, S. R. Arridge, and P. C. Beard, "Photoacoustic tomography with a limited-aperture planar sensor and a reverberant cavity," *Inverse Probl.* **23**(6), S95–112 (2007).
21. X. L. Deán-Ben et al., "Accurate model-based reconstruction algorithm for three-dimensional optoacoustic tomography," *IEEE Trans. Med. Imaging* **31**(10), 1922–1928 (2012).
22. C. Huang, A. A. Oraevsky, and M. A. Anastasio, "Investigation of limited-view image reconstruction in optoacoustic tomography employing a priori structural information," *Proc. SPIE* **7800**, 780004 (2010).
23. K. Wang et al., "Limited data image reconstruction in optoacoustic tomography by constrained, total variation minimization," *Proc. SPIE* **7899**, 78993U (2011).
24. B. T. Cox, S. R. Arridge, and P. C. Beard, "Estimating chromophore distributions from multiwavelength photoacoustic images," *J. Opt. Soc. Am. A* **26**(2), 443–455 (2009).
25. D. Razansky, J. Baeten, and V. Ntziachristos, "Sensitivity of molecular target detection by multispectral optoacoustic tomography (MSOT)," *Med. Phys.* **36**(3), 939–945 (2009).
26. J. Laufer et al., "Quantitative determination of chromophore concentrations form 2D photoacoustic images using a nonlinear model-based inversion scheme," *Appl. Opt.* **49**(8), 1219–1233 (2010).
27. G. Bal and K. Ren, "On multi-spectral quantitative photoacoustic tomography in a diffusive regime," *Inverse Probl.* **28**, 025010 (2012).
28. D. Razansky, A. Buehler, and V. Ntziachristos, "Volumetric real-time multispectral optoacoustic tomography of biomarkers," *Nat. Protoc.* **6**(8), 1121–1129 (2011).
29. D. Razansky, "Multispectral optoacoustic tomography: volumetric color hearing in real time," *IEEE Sel. Topics Quantum Electron.* **18**(3), 1234–1243 (2012).
30. A. V. Mamonov and K. Ren, "Quantitative photoacoustic imaging in radiative transport regime," *Commun. Math. Sci.* **12**(2), 201–234 (2014).
31. A. Pulkkinen et al., "A Bayesian approach to spectral quantitative photoacoustic tomography," *Inverse Probl.* **30**, 065012 (2014).
32. G. Bal and K. Ren, "Multi-source quantitative photoacoustic tomography in a diffusive regime," *Inverse Probl.* **27**, 075003 (2011).
33. T. Tarvainen et al., "Reconstructing absorption and scattering distributions in quantitative photoacoustic tomography," *Inverse Probl.* **28**, 084009 (2012).
34. A. Pulkkinen et al., "Approximate marginalization of unknown scattering in quantitative photoacoustic tomography," *Inverse Probl. Imag* **8**(3), 811–829 (2014).
35. B. Banerjee et al., "Quantitative photoacoustic tomography from boundary pressure measurements: noniterative recovery of optical absorption coefficient from the reconstructed absorbed energy map," *J. Opt. Soc. Am. A* **25**(9), 2347–2356 (2008).
36. B. T. Cox et al., "Two-dimensional quantitative photoacoustic image reconstruction of absorption distributions in scattering media by use of a simple iterative method," *Appl. Opt.* **45**, 1866–1875 (2006).
37. T. Jetzfellner et al., "Performance of iterative optoacoustic tomography with experimental data," *Appl. Phys. Lett.* **95**, 013703 (2009).
38. J. Ripoll and V. Ntziachristos, "Quantitative point source photoacoustic inversion formulas for scattering and absorbing media," *Phys. Rev. E* **71**, 031912 (2005).
39. L. Yao, Y. Sun, and H. Jiang, "Quantitative photoacoustic tomography based on the radiative transfer equation," *Opt. Lett.* **34**(12), 1765–1767 (2009).
40. L. Yao, Y. Sun, and H. Jiang, "Transport-based quantitative photoacoustic tomography: simulations and experiments," *Phys. Med. Biol.* **55**, 1917–1934 (2010).
41. A. Rosenthal, D. Razansky, and V. Ntziachristos, "Quantitative optoacoustic signal extraction using sparse signal representation," *IEEE Trans. Med. Imaging* **28**(12), 1997–2006 (2009).
42. W. Naetar and O. Scherzer, "Quantitative photoacoustic tomography with piecewise constant material parameters," *SIAM J. Imaging Sci.* **7**(3), 1755–1774 (2014).
43. B. Cox, T. Tarvainen, and S. Arridge, "Multiple illumination quantitative photoacoustic tomography using transport and diffusion models," in *Tomography and Inverse Transport Theory (Contemporary Mathematics)*, G. Bal et al., Eds., Vol. 559, pp. 1–12, American Mathematical Society, Providence (2011).
44. H. Gao, H. Zhao, and S. Osher, "Bregman methods in quantitative photoacoustic tomography," 2010, ftp://ftp.math.ucla.edu/pub/camreport/cam10-42.pdf (11 March 2015).
45. P. Shao, B. Cox, and R. Zemp, "Estimating optical absorption, scattering and Grueneisen distributions with multiple-illumination photoacoustic tomography," *Appl. Opt.* **50**(19), 3145–3154 (2011).
46. R. J. Zemp, "Quantitative photoacoustic tomography with multiple optical sources," *Appl. Opt.* **49**(18), 3566–3572 (2010).
47. T. Saratoon et al., "A gradient-based method for quantitative photoacoustic tomography using the radiative transfer equation," *Inverse Probl.* **29**, 075006 (2013).
48. K. Ren, H. Gao, and H. Zhao, "A hybrid reconstruction method for quantitative PAT," *SIAM J. Imaging Sci.* **6**(1), 32–55 (2013).
49. X. Li and H. Jiang, "Impact of inhomogeneous optical scattering coefficient distribution on recovery of optical absorption coefficient maps using tomographic photoacoustic data," *Phys. Med. Biol.* **58**, 999–1011 (2013).
50. D. J. Cuccia et al., "Modulated imaging: quantitative analysis and tomography of turbid media in the spatial-frequency domain," *Opt. Lett.* **30**(11), 1354–1356 (2005).
51. A. Joshi, W. Bangerth, and E. M. Sevick-Muraca, "Non-contact fluorescence optical tomography with scanning patterned illumination," *Opt. Express* **14**(14), 6516–6534 (2006).
52. A. Bassi et al., "Detection of inhomogeneities in diffusive media using spatially modulated light," *Opt. Lett.* **34**(14), 2156–2158 (2009).
53. C. D'Andrea et al., "Fast 3D optical reconstruction in turbid media using spatially modulated light," *Biomed. Opt. Express* **1**(2), 471–481 (2010).
54. A. Serdaroglu, B. Yazici, and K. Kwon, "Optimum source design for detection of heterogeneities in diffuse optical imaging," *Proc. SPIE* **6139**, 61391A (2006).
55. E. Zhang, J. Laufer, and P. Beard, "Backward-mode multiwavelength photoacoustic scanner using a planar Fabry-Perot polymer film ultrasound sensor for high-resolution three-dimensional imaging of biological tissue," *Appl. Opt.* **47**(4), 561–577 (2008).
56. J. Kaipio and E. Somersalo, *Statistical and Computational Inverse Problems*, Springer, New York (2005).
57. D. Calvetti and E. Somersalo, *Introduction to Bayesian Scientific Computing*, Springer, New York (2007).
58. T. Tarvainen et al., "Bayesian image reconstruction in quantitative photoacoustic tomography," *IEEE Trans. Med. Imaging* **32**(12), 2287–2298 (2013).
59. A. Ishimaru, *Wave Propagation and Scattering in Random Media*, Vol. 1, Academic Press, New York (1978).
60. T. Tarvainen et al., "Hybrid radiative-transfer-diffusion model for optical tomography," *Appl. Opt.* **44**(6), 876–886 (2005).
61. L. G. Henyey and J. L. Greenstein, "Diffuse radiation in the galaxy," *AstroPhys. J.* **93**, 70–83 (1941).
62. C. E. Rasmussen and C. K. I. Williams, *Gaussian Processes for Machine Learning*, MIT Press, Massachusetts (2006).

Aki Pulkkinen is a researcher at the University of Eastern Finland, Finland. He received his PhD degree from the University of Eastern Finland in 2014. His research interests include modeling of optical and ultrasonic propagation, therapeutic applications of ultrasound, and related inverse problems.

Ben T. Cox is a senior lecturer in the Photoacoustic Imaging Group within the Department of Medical Physics and Biomedical Engineering at University College London, United Kingdom. He received his PhD degree from the University of Southampton, United Kingdom,

in 1999. His research interests include photoacoustic imaging, numerical modeling of acoustics, and biomedical ultrasound.

Simon R. Arridge is a professor of image processing in the Department of Computer Science and visiting professor in the Department of Mathematics at University College London. He received his PhD degree from University College London in 1990. He has coauthored over 160 papers. His research interests include inverse problems in medical imaging, especially nonlinear tomography. He is the director of the UCL Centre for Inverse Problems and a member of the board of directors of the Centre for Medical Imaging.

Jari P. Kaipio is a professor of applied mathematics at the University of Auckland, New Zealand, and part-time professor of computational physics at the University of Eastern Finland, Finland. He received his PhD degree from the University of Kuopio, Finland, in 1996. He has coauthored over 140 papers and a book, *Statistical and Computational Inverse Problems*. His current research interests include inverse problems, especially Bayesian methods and nonstationary problems with various application areas.

Tanja Tarvainen is an academy research fellow at the University of Eastern Finland, Finland, and part-time research associate at University College London, United Kingdom. She received her PhD degree in 2006 from the University of Kuopio, Finland. Her current research interests include Bayesian approach to inverse problems with applications especially in optical tomographic methods.